

1 **Measurement report: Ambient volatile organic compounds (VOCs) pollution at urban**
2 **Beijing: characteristics, sources, and implications for pollution control**

3 Lulu Cui¹, Di Wu¹, Shuxiao Wang^{1,2*}, Qingcheng Xu¹, Ruolan Hu¹, Jiming Hao^{1,2}

4 ¹ *State Key Joint Laboratory of Environment Simulation and Pollution Control, School of Environment,*
5 *Tsinghua University, Beijing 100084, China*

6 ² *State Environmental Protection Key Laboratory of Sources and Control of Air Pollution Complex, Beijing*
7 *100084, China*

8 * Corresponding author. E-mail address: shxwang@tsinghua.edu.cn

9 **Abstract**

10 The increasing ozone (O₃) pollution and high fraction of secondary organic aerosols (SOA) in fine particle mass
11 highlighted the importance of volatile organic compounds (VOCs) in air pollution control. In this work, four
12 intensive field measurements of VOCs during winter of 2018 (from 1 December of 2018 to 17 January of 2019),
13 spring (15 April to 27 May), summer (17 June to 13 July) and autumn (22 September to 27 November) of 2019
14 were conducted at an urban site in Beijing to characterize VOCs sources and their contributions to air pollution.
15 The total mixing ratio of the 95 quantified VOCs (TVOC) observed in this study ranged from 5.5–118.7 ppbv
16 with the mean value of 34.9 ppbv. Alkanes, OVOCs and halocarbons were the dominant chemical groups,
17 accounting for 75-81% of the TVOCs across the sampling months. The molar ratios of VOCs to NO_x indicated
18 that O₃ formation was limited by VOCs during the whole sampling period. Positive matrix factorization (PMF)
19 analysis showed that diesel vehicle exhaust, gasoline vehicle exhaust and industrial emissions were the main
20 VOCs sources during both the O₃-polluted and PM_{2.5}-polluted months. On the base of O₃ formation impact,
21 VOCs from fuel evaporation and diesel exhaust particularly toluene, xylenes, trans-2-butene, acrolein, methyl
22 methacrylate, vinyl acetate, 1-butene and 1-hexene were the main contributors, illustrating the necessity of

23 conducting emission controls on these pollution sources and species for alleviating O₃ pollution. Instead, VOCs
24 from diesel exhaust and coal/biomass combustion were found to be the dominant contributors for secondary
25 organic aerosol formation potential (SOAFP), particularly the VOC species of toluene, 1-hexene, xylenes,
26 ethylbenzene and styrene, and top priority should be given to these for the alleviation of haze pollution. This
27 study provides insights for government to formulate effective VOCs control measures for air pollution in Beijing.

28 **Key words:** VOCs, OFP, SOAFP, Source appointment

29 **1. Introduction**

30 The ozone (O₃) and fine particulate matter (PM_{2.5}) pollution has restricted improvements in air quality in China.
31 Observation data from the Chinese Ministry of Environment and Ecology (MEE) network has witnessed an upward
32 trend for O₃ across the country over the period 2013-2019 (Fu et al., 2019; Li et al., 2017; Li et al., 2020; Shen
33 et al., 2019; Fan et al., 2020). Besides, haze pollution occurred in urban sites in recent years were commonly
34 characterized by enhanced formation of secondary organic aerosols (SOA) in fine particles, e.g., the fraction of
35 SOA in organic aerosols reached 58% in Xi'an during winter 2018 and 53% in urban Beijing during winter
36 2014 (Kuang et al., 2020; Li et al., 2017b; Sun et al., 2020; Xu et al., 2019). Volatile organic compounds (VOCs)
37 are key precursors for the formation of O₃ via gas-phase reactions (Odum et al., 1997; Atkinson, 2000; Sato et
38 al., 2010; Huang et al., 2014). In highly polluted urban regions, the O₃ formation was generally VOCs-limited,
39 and it is suggested that VOCs emission control is necessary for effective alleviation of photochemical smog (Liu
40 et al., 2020a,b; Shao et al., 2009; Wang et al., 2020; Xing et al., 2011). Besides, the VOCs compounds including
41 aromatics and biogenic species have significant impact on SOA formation which play an important role in haze
42 formation (Huang et al., 2014; Tong et al., 2021). VOCs emission abatement is therefore imperative for
43 improving air quality in China.

44 VOCs in ambient air can be emitted by a variety of sources including both anthropogenic and biogenic
45 sources. While biogenic emissions are significantly greater than anthropogenic emissions globally (Dombia et
46 al., 2021; Sindelarova et al., 2022), anthropogenic emissions play the dominant role in urban and surrounding
47 areas (Warneke et al., 2007; Ahmad et al., 2017; Wu and Xie, 2018). The VOC observations in China showed
48 distinct differences in anthropogenic sources among different regions. For example, solvent use and vehicle
49 exhaust are primary VOCs sources in urban Shanghai and urban Guangzhou, while the primary sources of VOCs

50 in Wuhan, Zhengzhou and Beijing cities are combustion and vehicle exhaust (Han et al., 2020; Shen et al., 2020;
51 Liu et al., 2020a; Li et al., 2019a). Apart from the diversity of emission sources, different VOCs species exhibited
52 different propensities to form O₃ and SOA. Observation-based studies commonly applied the O₃ formation
53 potential (OFP) and SOA formation potential (SOAFP) scales to quantify the relative effects of specific VOCs
54 and sources on O₃ and SOA formation and to aid in the development of efficient control strategies (Carter and
55 Atkinson, 1989; Chang and Rudy, 1990; Han et al., 2020; Zhang et al., 2017). Although there have been many
56 studies on ambient VOCs in various locations (e.g., urban, rural, and industrial areas), most of these
57 measurements were confined to short periods (a few days or a certain season), and the understanding of temporal
58 variations of concentrations, sources as well as the influence of photochemical reactions of VOCs on annual scale
59 was still limited. Besides, most of the available reports on VOCs analysis based on online analytical techniques
60 include mainly non-methane hydrocarbon compounds, and thus the characteristics of VOCs as well as their
61 relationships with PM_{2.5} and O₃ cannot be fully revealed since OVOC also participate actively in chemical
62 reactions related to secondary formation (Li et al., 2019a; Zhao et al., 2020; Yang et al., 2018; Sinha and Sinha.,
63 2019). Therefore, the long-term and comprehensive monitoring of VOCs are desired.

64 As the capital and one of the largest megacities in China, Beijing has been suffering from severe O₃ pollution
65 due to rapid economic development and increases in precursor emissions (Wang et al., 2014a; Wang et al, 2017;
66 Li et al., 2019d; Zhao et al., 2020). According to the Report on the State of the Ecology and Environment in
67 Beijing, the average 90th percentile O₃ daily maximum 8 h concentration in Beijing exceeded the national
68 standards, reaching 193, 192, and 191 µg/m³ in 2017, 2018, and 2019, respectively. In addition, the number of
69 motor vehicles in Beijing reached 6.365 million at of the end of 2019 (<http://beijing.gov.cn>), making Beijing the
70 top city in China in terms of number of motor vehicles. The existing field measurements in Beijing were mostly

71 conducted before 2016, and the observation in most recent years is quite limited (Li et al., 2015; Li et al., 2019c;
72 Liu et al., 2020a; Yang et al., 2018). In this work, ambient air samples were collected at an urban site in Beijing
73 from December 2018 to mid-January 2019, mid-April to late May 2019, mid-June to mid-July 2019, and late
74 September to late November 2019, respectively. Several O₃ and PM_{2.5} pollution events were captured during the
75 sampling period. The characteristics and the contribution of specific species and sources of VOCs on O₃ and SOA
76 formation, with a focus on photochemical and haze pollution periods, were analyzed in detail. The results and
77 implications from this study can provide useful guidance for policymakers to alleviate ozone and haze pollution in
78 Beijing.

79 **2. Methodology**

80 **2.1 Field measurement**

81 The sampling site is at the roof of a three-floor building on the campus of Tsinghua University (40.00°N,
82 116.33°E), northwest of Beijing urban area (Fig. S1). The altitude of the sampling site is 57 m. This sampling
83 site is surrounded by school and there are no large emission sources nearby, therefore it can represent the urban
84 air quality in Beijing. Details of the site description is found in Xu et al., (2019).

85 The air samples were collected using 6 L summa canisters (Entech, USA) with a stable rate of 4.26 ml/min.
86 The samples were pre-processed to remove N₂, O₂, CO₂, CO and H₂O in the samples and to further concentrate
87 the samples in volume by the cryogenic pre-concentrator (Model 7100, Entech Instruments Inc., USA). Pressure
88 gage was used to test if the canister has air leakage exist before sampling every time, and blanks were prepared
89 using cleaned canisters to fill with high purity nitrogen. The cryotrap of precooling system was baked before
90 analyses each day and between every samples. The VOCs in air samples were analyzed by a gas chromatography
91 system that was equipped with a mass spectrometric detector (GC-MS) (Agilent Tech., 7890/5975, USA). The

92 suitability of this system for VOCs measurement are well verified and it has been used in field campaigns (Li et
93 al., 2014; Wu et al., 2016). The oven temperature was programmed at 40 °C for 3 minutes initially, then raised
94 to 90 °C at 8°C per minute, and later raised to 220 °C at 6°C per minute, holding for 9 minutes. In this work, 95
95 target VOCs, including 25 alkanes, 8 alkenes, 16 aromatics, 34 halocarbons and 12 OVOC were quantified. It
96 should be noted that VOCs compounds (C2-C3) with low boiling point (i.e., ethane, ethene, acetylene,
97 and propane) were not detected by the GC-MS system. The standard substance (SPECTRA GASES Inc., USA)
98 mentioned for Photochemical Assessment Monitoring Stations (PAMS) and US EPA TO-15 standard was used
99 to construct the calibration curves for the target VOCs. Quality assurance and quality control, including method
100 detection limit (MDL) of each compound, laboratory and field blanks, retention time, accuracy and duplicate
101 measurements of samples were performed according to USEPA Compendium Method TO-15 (USEPA 1999).
102 The correlated coefficients of the calibration curves for all the compounds were > 0.95. The relative standard
103 deviation (RSD) for all of compounds of triplicates were 0.5%-6.0%. Previous field measurements have
104 reported that the precision of GC-MS system for hydrocarbons and aldehydes was below 6% and 15%,
105 respectively (Li et al., 2014; Wu et al., 2016). In this work, one kind of aldehyde substance, i.e., acrolein was
106 detected, with R² and RSD of 0.99 and 4.5%, respectively.

107 During the sampling periods, the measurements of PM_{2.5}, gaseous pollutants (NO_x and O₃), and
108 meteorological variables (such as temperature, relative humidity, wind speed, and wind direction) were
109 conducted simultaneously. SO₂, NO_x and O₃ were analyzed using the the Pulsed Fluorescence SO₂ Analyzer
110 (Thermo Fisher Scientific USA, 43I), Chemiluminescence NO–NO₂–NO_x Analyzer (Thermo Fisher Scientific
111 USA, 17I) and ultra-violet (UV) photometric O₃ Analyzer (Thermo Fisher Scientific USA, 49I) , respectively.
112 The mass concentration of PM_{2.5} was measured using an oscillating balance analyzer (TH-2000Z, China) (Wang

113 et al., 2014a). The quality assurance of SO₂, NO₂, O₃, and PM_{2.5} was conducted based on HJ 630-2011
114 specifications. Meteorological variables including wind speed (WS), wind direction (WD), relative humidity
115 (RH), air pressure, temperature, and precipitation were measured by an automatic weather monitoring system.
116 The planetary boundary height was obtained from the European Centre for Medium-Range Weather Forecasts
117 (<https://www.ecmwf.int/en/forecasts/datasets/browse-reanalysis-datasets>).

118 **2.2 Ozone formation potential (OFP) and secondary formation potential (SOAFP) calculation**

119 The formation potential of O₃ and SOA was used to characterize the relative importance of VOCs species and
120 sources in secondary formation, which were estimated using Eqs. (1) and (2).

$$121 \quad OFP = \sum_i^n MIR_i \times [VOC(ppb)]_i \quad (1)$$

$$122 \quad SOAFP = \sum_i^n Y_i \times [VOC(ppb)]_i \quad (2)$$

123 where n represents the number of VOCs, $[VOC]_i$ represents the i th VOC species concentration, MIR_i is the
124 maximum incremental reactivity for the i th VOC species, and Y_i is the SOA yield of VOC _{i} (McDonald et al.,
125 2018). The MIR for each VOC species were taken from the updated Carter research results
126 (<http://www.engr.ucr.edu/~carter/reactdat.htm>, last access: 24 February 2021). For species lacking yield curves,
127 the fractional aerosol coefficient (FAC) values proposed by Grosjean and Seinfeld (1989) were used.

128 **2.3 Deweathered model**

129 In this work, the influences of meteorological conditions on O₃ and PM_{2.5} were removed using the random forest
130 (RF) model. The meteorological predictors in the RF model include wind speed (WS), wind direction (WD), air
131 temperature (T), relative humidity (RH), precipitation ($Prec$), air pressure (P), time predictors (year, day of year
132 (DOY), hour) and planetary boundary layer height (BLH). These meteorological parameters have been reported
133 to be strongly associated with PM_{2.5} and O₃ concentrations in various regions in China (Chen et al., 2020; Feng

134 et al., 2020) and contributed significantly in previous PM_{2.5} and O₃ prediction models (She et al., 2020; Li et al.,
135 2020). The modelling relates the hourly variability of O₃ and PM_{2.5} to that of meteorological variables. The model
136 performance was evaluated through 10-fold cross validation (CV) approach, which randomly selects 10% of the
137 dataset for model testing and trains the model with the remaining data. This process was repeated ten times, and
138 each record was selected once as testing data. In each round, the training dataset includes ~90% randomly selected
139 data representing different seasons. After the building of the RF model, the deweathered technique was applied
140 to predict the air pollutant level at a specific time point. The differences in original pollutant concentrations and
141 deweathered pollutant concentrations were regarded as the concentrations contributed by meteorology. Statistical
142 indicators including R^2 , RMSE, and MAE values were regarded as the major criteria to evaluate the modeling
143 performance.

144 **2.4 Positive matrix factorization (PMF)**

145 In this study, the US EPA PMF 5.0 software was used for VOCs source apportionment (Abeira et al., 2017; Li
146 et al., 2019a; Xue et al., 2017). The detailed description of the PMF model is found elsewhere (Ling et al., 2011;
147 Yuan et al., 2009). PMF uses both concentration and user-provided uncertainty associated with the data to weight
148 individual points. Species with high percentages of missing values (> 40 %) and with signal-to-noise ratio of
149 below 2 were excluded. Based on this, 53 VOC species including source tracers (e.g., chloromethane,
150 trichloroethylene, tetrachloroethylene and MTBE) and SO₂ were chosen for the source apportionment analysis.
151 Data values below the MDL were replaced by MDL/2, and the missing data were substituted with median
152 concentrations. If the concentration is less than or equal to the MDL provided, the uncertainty is calculated using
153 the equation of $Unc = 5/6 \times MDL$; if the concentration is greater than the MDL provided, the uncertainty is
154 calculated as $Unc = [(error\ factor \times mixing\ ratio)^2 + (MDL)^2]^{1/2}$.

155 During the PMF analysis, the bootstraps (BS) method, displacement (DISP) analysis, and the combination
156 of the DISP and BS (BS–DISP) were used to evaluate the uncertainty of the base run solution. A total of 100
157 bootstrap runs were performed, and acceptable results were gained for all factors (above 90%). Based on the
158 DISP analysis, the observed drop in the Q value was below 0.1 %, and no factor swap occurred, confirming that
159 the solution was stable. The BS–DISP analysis showed that the observed drop in the Q value was less than 0.5 %,
160 demonstrating that the solution was useful.

161 **3. Results and discussion**

162 **3.1 TVOC mixing ratios and chemical composition**

163 The time series of meteorological parameters and concentrations of air pollutants during the measurement period
164 are shown in Fig. 1. The ambient temperature ranged from -13.3°C to 38.7°C and the RH varied between 5% and
165 99% across the sampling months. Prevailing winds shifted between southwesterly and northeasterly with WS of
166 0–6.8 m s⁻¹. The mixing ratio of total VOCs (TVOC) ranged from 5.5–118.7 ppbv during the sampling period
167 with relatively higher values during September and November (49.9-51.6 ppbv) while relatively lower values
168 (22.2-27.5 ppbv) across the other months. Major VOC compositions were generally consistent during the whole
169 measurement period. Alkanes, OVOCs and halocarbons were the dominant chemical groups, accounting for 75-
170 81% of the TVOCs across the sampling months. In terms of individual species, acetone, dichloromethane, n-
171 butane, toluene, methyl tert butyl ether (MTBE), iso-pentane, propylene, n-hexane, 1,1-dichloroethane, benzene
172 and 1-butene made up the largest contribution, accounting for 50.6 % of the TVOC on average during the whole
173 measurement period.

174 As shown in Fig. 2, the concentrations of TVOCs and major VOC groups including alkanes, alkenes,
175 aromatics, halocarbons and OVOCs observed in this study were apparently lower than those during the sampling

176 months in 2014 and 2016 in urban Beijing (An et al., 2012; Liu et al., 2020a; Li et al., 2015b), indicating the
177 effectiveness of control measures in most recent years on lowering VOCs emission. Besides, the composition of
178 major chemical groups also showed remarkable changes, with decreased proportions of alkanes while increased
179 fractions of halocarbons, aromatics and OVOCs, reflecting the changes in emission sources types in most recent
180 years.

181 During the measurement period, 14 O₃ pollution episodes (days with maximum 8-h average O₃ exceeding
182 160 μg m⁻³) were observed on 17 April, 3-4 May, 16 May, 19-20 June, 24-25 June, 2 July, 5 July, 13 July, 25-26
183 September and 28 September of 2019, respectively. The comparison of meteorological parameters and air
184 pollutants on O₃ pollution and compliance days (days with maximum 8-h average O₃ below 160 μg m⁻³) during
185 the five O₃-polluted months (i.e., April, May, June, July, and September of 2019) is discussed here. As shown in
186 Fig. 3, the WS on O₃ pollution days ($1.31 \pm 0.90 \text{ m s}^{-1}$) was slightly lower than that on O₃ compliance days (1.47
187 $\pm 1.10 \text{ m s}^{-1}$), indicating that precursors were more conducive to be diluted on O₃ compliance days. The variation
188 trend of O₃ and temperature displayed the negative correlation, and the linear correlations between O₃ and
189 temperature on O₃ pollution days ($R^2 = 0.63$) was stronger than that on O₃ compliance days ($R^2 = 0.35$). The mean
190 TVOC concentration on O₃ pollution days (32.3 ppbv) was higher than that on O₃ compliance days (29.6 ppbv),
191 which was mainly attributed to higher concentrations of MTBE, acrolein, trans-2-butene r on pollution days.
192 MTBE is widely used as a fuel additive in motor gasoline (Liang et al., 2020), and trans-2-butene is the main
193 component of oil/gas evaporation (Li et al., 2019a). Such result suggested enhanced contribution of traffic
194 emissions on O₃ pollution days. Besides, the concentration of isoprene, which is primarily produced by vegetation
195 through photosynthesis, increased significantly on O₃ pollution days probably due to the stronger plant emission
196 at elevated temperature (Guenther et al., 1993, 2012; Stavrou et al., 2014). The ratio of *m/p*-xylene to

197 ethylbenzene (X/E) measured can be used as an indicator of the photochemical aging of air masses because of
198 their similar sources in urban environments and differences in atmospheric lifetimes (Carter., 2010; Miller et al.,
199 2012; Wang et al., 2013a). The mean X/E value on O₃ compliance days (1.41) was higher than that on O₃ pollution
200 days (1.17), indicating enhanced secondary transformation of VOCs on O₃ pollution days.

201 The daily PM_{2.5} concentrations ranged from 9-260 µg m⁻³ with the mean value of 88.5 µg m⁻³ during the
202 measurement period. 15 PM_{2.5} pollution days (daily average PM_{2.5} exceeding 75 µg m⁻³) were observed on 3
203 January, 12-13 January, 22-23 April, 29 April, 12 May, 15 May, 19 October, 21-23 November of 2019, 1-2
204 December and 5 December of 2018, respectively. During the six PM_{2.5}-polluted months (i.e., December of 2018,
205 January, April, May, October and November of 2019), the WS on PM_{2.5} pollution days (1.05 ± 1.06 m s⁻¹) was
206 lower than that on PM_{2.5} compliance days (1.43 ± 1.06 m s⁻¹), indicating the weaker ability of winds for the
207 dilution and diffusion of precursor on PM_{2.5} pollution days. The mean X/E value on PM_{2.5} compliance days (1.47)
208 was slightly higher than that on PM_{2.5} pollution days (1.44), indicating enhanced secondary transformation of
209 VOCs on PM_{2.5} pollution days.

210 **3.2 The role of VOCs on secondary pollution**

211 **3.2.1 Estimating O₃ and PM_{2.5} levels contributed by emissions**

212 O₃ and secondary aerosols are primarily formed via photochemical reactions in the atmosphere, of which
213 concentrations could be largely influenced by meteorological conditions (Chen et al., 2020; Feng et al., 2020;
214 Zhai et al., 2019). In this work, the respective contributions of meteorology and emissions to PM_{2.5} and O₃
215 variations were determined using the RF model as described in section 2.3. The coefficients of determination (R^2)
216 for the RF model in predicting PM_{2.5} and O₃ are 0.85 and 0.91, respectively (Shown in Fig. S2). The respective
217 contributions of anthropogenic and meteorology to O₃ and PM_{2.5} during each period is shown in Fig. 4. During

218 the O₃-polluted months, the meteorologically-driven O₃ level on O₃ pollution days (72.5 μg m⁻³) was significantly
219 higher than that on O₃ compliance days (35.3 μg m⁻³). After removing the meteorological contribution, the
220 residual emission-driven O₃ level on O₃ pollution (45.3 μg m⁻³) and compliance days (44.9 μg m⁻³) of the O₃-
221 polluted months was almost identical and were significantly higher than that during the non-O₃-polluted months
222 (23.8 μg m⁻³). The emission-driven PM_{2.5} level was in the order of: PM_{2.5} pollution days of the PM_{2.5}-polluted
223 months (55 μg m⁻³) > PM_{2.5} compliance days of the PM_{2.5}-polluted months (44 μg m⁻³) > non-PM_{2.5}-polluted
224 months (29 μg m⁻³). These results suggested that apart from meteorological factors, emissions also play a role in
225 deteriorating PM_{2.5} and O₃ pollution, and reducing anthropogenic emissions is essential for improving air quality.

226 The VOCs/NO_x ratio has been widely used to distinguish whether the O₃ formation is VOC limited or NO_x
227 limited (Li et al., 2019a). Generally, VOC-sensitive regime occurs when VOCs/NO_x ratios are below 10 while
228 NO_x-sensitive regime occurs when VOCs/NO_x ratios are higher than 20 (Hanna et al., 1996; Sillman, 1999). In
229 this study, the values of VOCs/NO_x (ppbv ppbv⁻¹) were all below 3 during both the O₃-polluted and non-O₃-
230 polluted months (Fig. S3), suggesting that the O₃ formation was sensitive to VOCs, and thus the reductions of
231 the emissions of VOCs will be beneficial for O₃ alleviation.

232 **3.2.2 Contribution of VOCs to OFP and SOAFP**

233 As discussed in 3.1, O₃ formation was generally VOCs-sensitive during the measurement period. Quantifying the
234 contribution of speciated VOCs species to O₃ is helpful for developing effective VOCs control measures and
235 alleviating O₃ pollution. The averaged OFP on O₃ pollution days of the O₃-polluted months, O₃ compliance days
236 of the O₃-polluted months, and during the non-O₃-polluted months were 224.9, 201.4, and 187.5 μg m⁻³,
237 respectively (Fig. 5). According to our observations, the higher OFP on O₃ pollution days than that on O₃
238 compliance days during the O₃-polluted months was mainly attributed to higher levels of trans-2-butene, o-xylene

239 and acrolein O₃ on pollution days, in line with that in Fig. 3. Alkenes, aromatics and OVOCs were the three
240 biggest contributors to O₃ formation, accounting for 85.1%, 85.7% and 81.6% of the total OFP on O₃ pollution
241 days of the O₃-polluted months, O₃ compliance days of the O₃-polluted months, and during the non-O₃-polluted
242 months, respectively. In terms of the individual species, the top 10 highest contributors during the O₃-polluted
243 months were toluene (6.4% and 7.5% on O₃ pollution and compliance days, respectively), trans-2-butene (9.6%
244 and 7.5%), acrolein (10.8% and 5.7%), m/p-xylene (6.1% and 6.9%), o-xylene (6.6% and 5.8%), 1-butene (5.2%
245 and 7.1%), 1-hexene (4.4% and 5.4%), vinyl acetate (4.2% and 5.7%), methyl methacrylate (5.5% and 4.8%),
246 and 1-pentene (4.5% and 4.4%). During the non-O₃-polluted months, the overall OFP was mainly contributed
247 by toluene (10.8%), trans-2-butene (10.5%), 1-butene (7.3%), m/p-xylene (6.5%), 1-pentene (5.7%), 1-hexene
248 (5.0%), methyl methacrylate (4.9%), o-xylene (4.9%), vinyl acetate (3.8%), and isopentane (2.3%), respectively.

249 As shown in Fig. S3, the ratio of VOCs/NO_x was generally below 3 during the sampling period, indicating
250 high NO_x conditions. Based on the estimated yields of the VOCs shown in Table S2, the SOAFPs were calculated
251 and compared in Fig. 5. The mean SOAFP on PM_{2.5} pollution days of the PM_{2.5}-polluted months, PM_{2.5}
252 compliance days of the PM_{2.5}-polluted months, and during the non-PM_{2.5}-polluted months were 1.28, 1.07, and
253 0.89 μg m⁻³. During the six PM_{2.5}-polluted months, the higher SOAFP on PM_{2.5} pollution days than that on PM_{2.5}
254 compliance days was mainly attributed to higher levels of 1,2,4-trimethylbenzene, n-undecane, n-nonane, 1,4-
255 diethylbenzene, and 1,3-diethylbenzene on PM_{2.5} pollution days. Aromatics have the largest SOAFP, accounting
256 for 74% and 75% of the total SOAFP on PM_{2.5} pollution and compliance days of the PM_{2.5}-polluted months, and
257 70% of the total SOAFP during the non-PM_{2.5}-polluted months, respectively. The 10 species responsible for most
258 of the SOAFP were toluene (41% and 40% on PM_{2.5} pollution and compliance days of the PM_{2.5}-polluted months,
259 and 33% during the non-PM_{2.5}-polluted months), 1-hexene (13.0%, 12.5%, and 15.2%), xylenes (11.6%, 14.1%

260 and 14.8%), ethylbenzene (4.9%, 5.3% and 6.0%), styrene (4.5%, 5.6% and 5.6%), 1-pentene (3.3%, 3.4% and
261 4.3%), methyl cyclopentane (2.1%, 2.7% and 3.6%), 1,2,3-trimethylbenzene (2.8%, 2.4% and 2.8%), m-ethyl
262 toluene (1.7%, 1.4% and 1.7%) and p-ethyl toluene (1.7%, 1.4% and 1.7%), respectively.

263 **3.3 Source apportionment of VOCs**

264 **3.3.1 Indication from tracers**

265 The great changes in the mixing ratios of different species are mainly affected by the photochemical processing
266 and the emission inputs, and ratios of VOCs species having similar atmospheric lifetimes can reflect the source
267 features (Li et al., 2019a; Raysoni et al., 2017 Song et al., 2021). The ratio of *i*-pentane to *n*-pentane are widely
268 used to examine the impact of vehicle emissions, fuel evaporation and combustion emissions, within the *i/n*-
269 pentane ratios of ranging between 2.2–3.8, 1.8–4.6 and 0.56-0.80, respectively (McGaughey et al., 2004; Jobson
270 et al., 2004; Russo et al., 2010; Wang et al., 2013b; Yan et al., 2017). As shown in Fig. 6, the *i/n*-pentane ratios
271 during the PM_{2.5}-polluted months were mostly within the range of 0.3-2.0, suggesting the pentanes were from
272 the mixed sources of coal combustion and fuel evaporation. During the non-PM_{2.5}-polluted months, the *i/n*-
273 pentane ratios were distributed in the range of 1.3-3.4, indicating strong impacts from vehicle exhaust and fuel
274 evaporation. During the O₃-polluted months, most of the *i/n*-pentane ratios (1.5-2.5) were distributed within the
275 reference range of vehicle exhaust and fuel evaporation, whereas most of the *i/n*-pentane ratios during the non-
276 O₃-polluted months ranged between 1.7-2.1, suggesting the significant impact of fuel evaporation.

277 The toluene/benzene (T/B) ratio, a widely used indicator for sources of aromatics. In areas heavily impacted
278 by vehicle emissions, the T/B ratio lies in the range of 0.9–2.2 (Qiao et al., 2012; Dai et al., 2013; Wang et al.,
279 2013c; Yao et al., 2013; Zhang et al., 2013; Yao et al., 2015a; Mo et al., 2016; Deng et al., 2018). Higher T/B
280 ratios were reported for solvent use (greater than 8.8) (Yuan et al., 2010; Wang et al., 2014b; Zheng et al., 2013)

281 and industrial processes (1.4-5.8) (Mo et al., 2015; Shi et al.,2015). In burning source emission studies, the T/B
282 ratio was below 0.6 in different combustion process and raw materials (Tsai et al., 2003; Akagi et al., 2011; Mo
283 et al., 2016). Most of the T/B ratios during the PM_{2.5}-polluted and non-PM_{2.5}-polluted months were within the
284 range of 1.1-1.8 and 0.8-2.2, whereas the T/B ratios were mostly distributed within the range of 0.8-2.2 and 0.9-
285 1.9 during the O₃-polluted and non-O₃-polluted months, respectively, suggesting the significant impact of vehicle
286 and industrial emissions.

287 **3.3.2 PMF**

288 The factor profiles given by PMF and the contribution of each source to ambient VOCs during each period is
289 presented in Fig. 7 and Fig. 8, respectively. Six emission sources were identified: coal/biomass burning, solvent
290 use, industrial sources, oil gas evaporation, gasoline vehicle emission, and diesel vehicle emission based on the
291 corresponding markers for each source category. In general, diesel vehicle exhaust, gasoline vehicle exhaust and
292 industrial emissions were the main VOCs sources during both the O₃-polluted and PM_{2.5}-polluted months, with
293 total contributions of 62% and 62% on O₃ pollution and compliance days of the O₃-polluted months, and 66%
294 and 59% on PM_{2.5} pollution and compliance days of the PM_{2.5}-polluted months, respectively. The O₃-polluted
295 months exhibited higher proportions of diesel (24% on O₃ compliance days and 27% on O₃ pollution days) and
296 gasoline vehicle emission (17% on O₃ compliance days and 16% on O₃ pollution days) compared with the non-
297 O₃-polluted months (8% and 13%, respectively). During the O₃-polluted months, the contributions of industrial
298 emissions (22%) and fuel evaporation (18%) on O₃ pollution days were much higher than those on O₃ compliance
299 days (18% and 13%, respectively). Figure 9 presents the relative contributions of individual VOC sources from
300 PMF to OFP. On the base of O₃ formation impact, diesel and gasoline vehicle exhaust were major contributors.
301 During the O₃-polluted months, vehicle emissions and fuel evaporation showed higher OFP values on O₃

302 pollution days (93.9 and $35.5 \mu\text{g m}^{-3}$) compared with those on O_3 compliance days (88.0 and $25.8 \mu\text{g m}^{-3}$,
303 respectively). Although industrial emissions act as an important source for VOCs concentrations on O_3 -pollution
304 days (shown in Fig. 8), the potential to form O_3 is limited, accounting for 11% of the total OFP. As illustrated in
305 Fig.7, the industrial source was distinguished by high compositions of alkanes while relatively lower
306 compositions of alkenes and aromatics, resulting in low O_3 formation potentials. Such results suggested that the
307 fuel use and diesel vehicle exhaust should be controlled preferentially for O_3 mitigation.

308 The $\text{PM}_{2.5}$ -polluted months showed higher proportions of industrial (29% on both $\text{PM}_{2.5}$ compliance and
309 $\text{PM}_{2.5}$ pollution days) and coal/biomass combustion emissions (16% on $\text{PM}_{2.5}$ compliance days and 18% on $\text{PM}_{2.5}$
310 pollution days) compared with the non- $\text{PM}_{2.5}$ -polluted months (17% and 10%, respectively). The $\text{PM}_{2.5}$ pollution
311 days were dominated by industrial emission (29%), diesel vehicle exhaust (24%), and combustion source (18%).
312 During the $\text{PM}_{2.5}$ -polluted months, the contribution of diesel vehicle exhaust on $\text{PM}_{2.5}$ pollution days (24%) was
313 higher than that on $\text{PM}_{2.5}$ compliance days (16%). On the base of $\text{PM}_{2.5}$ formation impact, diesel vehicle exhaust
314 and combustion were two major contributors on $\text{PM}_{2.5}$ pollution days (shown in Fig. 9), and these two sources
315 showed obvious higher SOAFP on $\text{PM}_{2.5}$ pollution days (0.30 and $0.32 \mu\text{g m}^{-3}$, respectively) compared with those
316 on $\text{PM}_{2.5}$ compliance days of the $\text{PM}_{2.5}$ -polluted months (0.15 and $0.14 \mu\text{g m}^{-3}$, respectively). Although industrial
317 emissions act as an important source for VOCs concentrations on $\text{PM}_{2.5}$ pollution days, the potential to form $\text{PM}_{2.5}$
318 is limited, accounting for 16% of the total SOAFP. The above results suggested that diesel vehicle exhaust and
319 combustion should be controlled preferentially for alleviating $\text{PM}_{2.5}$ pollution.

320 Based on the mass concentrations of individual species in each source, m/p-xylene, o-xylene, methyl
321 methacrylate, vinyl acetate, 1-hexene, and acrolein in gasoline and diesel vehicular emissions; toluene, trans-2-
322 butene, and 1-pentene in fuel evaporation and diesel vehicular emissions; acrolein in solvent, gasoline vehicular

323 and diesel vehicular emissions were the dominant species contributing to photochemical O₃ formation (Fig. 10).
324 Toluene, m/p-xylene, o-xylene, styrene, ethylbenzene, 1-pentene, 1,2,3-trimethylbenzene from combustion and
325 diesel vehicular emissions; 1-hexene from diesel vehicular emission; and methyl cyclopentane from combustion,
326 industrial and diesel vehicular emissions were the dominant contributors for SOA formation during the PM_{2.5}
327 pollution periods (Fig. 10).

328 **3.4 Limitation**

329 This study analyzed the VOC sources and their contributions to O₃ and SOA formation across different seasons.
330 It should be pointed out that the sampling campaign for VOCs measurement was not conducted continuously
331 during December 2018 and November 2019. For instance, the air samples were not collected in August and
332 February-March of 2019, during which the pollution events of O₃ and PM_{2.5} occurred, respectively. The variations,
333 sources and secondary transformation potentials of VOCs, particularly for O₃ and PM_{2.5} pollution periods cannot
334 be fully depicted. Despite the uncertainties that remained, the results obtained in this study provide useful
335 information for VOCs emission control strategy and assist overcoming air pollution issue in Beijing.

336 **4. Conclusions**

337 In this work, the field sampling campaign of VOCs was conducted at urban Beijing from December 2018 to
338 November 2019. The VOCs concentrations ranged from 5.5 to 118.7 ppbv with mean value of 34.9 ppbv. Alkanes,
339 OVOCs and halocarbons were the dominant chemical groups, accounting for 75-81% of the TVOCs across the
340 sampling months. By excluding the meteorological impact, the emission-driven O₃ level during the O₃-polluted
341 months were higher than that during the non-O₃-polluted months, and similar pattern was found for PM_{2.5}. The
342 molar ratio of VOCs to NO_x indicated that O₃ formation was limited by VOCs during both the O₃-polluted non-
343 O₃-polluted months, and thus reducing VOCs emission is essential for alleviation of O₃ pollution. The

344 contributions of coal/biomass combustion, solvent use, industrial sources, oil/gas evaporation, gasoline exhaust,
345 and diesel exhaust were identified based on PMF analysis. Considering both the concentration and maximum
346 incremental reactivity of individual VOC species for each source, fuel use and diesel exhaust sources were
347 identified as the main contributors of O₃ formation during the O₃-polluted months, particularly the VOCs species
348 of toluene, xylenes, trans-2-butene, acrolein, methyl methacrylate, vinyl acetate, 1-butene and 1-hexene,
349 illustrating the necessity of conducting emission controls on these pollution sources and species for alleviating
350 O₃ pollution. VOCs from diesel vehicles and combustion were found to be the dominant contributors for SOAFP,
351 particularly the VOC species of toluene, 1-hexene, xylenes, ethylbenzene and styrene, and top priority should be
352 given to these for the alleviation of haze pollution.

353 **Data availability**

354 The meteorological data are available at <http://data.cma.cn/> (China Meteorological Administration). The website
355 can be browsed in English <http://data.cma.cn/en>. The concentrations of air pollutants including PM_{2.5}, O₃ and
356 NO_x are available at <https://air.cnemc.cn:18007/> (Ministry of Ecology and Environment the People's Republic of
357 China). The website can be browsed in English <http://english.mee.gov.cn/>. The daily mixing ratio of individual
358 VOCs species is given in Table S1 in the Supplement.

359 **Author Contributions**

360 DW designed the study and performed the VOCs measurement. QX and RH assists in air sampling and data
361 collection. LC performed the data analysis and wrote the paper with contributions from all co-authors. SW and
362 JH reviewed the paper and provided comments for improving the paper.

363 **Competing interests**

364 The authors declare that they have no conflict of interest.

365 **Acknowledgements**

366 This work was supported by the National Natural Science Foundation of China (92044302) and the Beijing

367 Municipal Science and Technology Project (Z211100004321006 & Z191100009119001).

368 **References**

- 369 Abeleira, A., Pollack, I. B., Sive, B., Zhou, Y., Fischer, E. V., Farmer, D. K., 2017. Source characterization of
370 volatile organic compounds in the Colorado Northern Front Range Metropolitan Area during spring and summer
371 2015, *J. Geophys. Res.-Atmos.*, 122, 3595–3613, <https://doi.org/10.1002/2016jd026227>.
- 372 Ahmad, W., Coeur, C., Tomas, A., Fagniez, T., Brubach, J. B., Cuisset, A., 2017. Infrared spectroscopy of
373 secondary organic aerosol precursors and investigation of the hygroscopicity of SOA formed from the OH
374 reaction with guaiacol and syringol. *Appl. Opt.* 56, E116, <https://doi.org/10.1364/AO.56.00E116>. Akagi, S. K.,
375 Yokelson, R. J., Wiedinmyer, C., Alvarado, M. J., Reid, J. S., Karl, T., Crounse, J. D., Wennberg, P. O., 2011.
376 Emission factors for open and domestic biomass burning for use in atmospheric models. *Atmos. Chem. Phys.* 11,
377 4039–4072.
- 378 Atkinson, R., 2000. Atmospheric chemistry of VOCs and NO_x. *Atmos. Environ.* 34, 2063–2101.
- 379 An, J.L., Wang, Y.S., Wu, F.K., Zhu, B., 2012. Characterizations of volatile organic compounds during high
380 ozone episodes in Beijing, China. *Environ. Monit. Assess.* 184, 1879e1889.
- 381 Carter, W.P.L. and Atkinson, R., 1989. Computer modeling study of incremental hydrocarbon reactivity. *Environ.*
382 *Sci. Technol.* 23, 864–880, <https://doi.org/10.1021/es00065a017>.
- 383 Carter, W.P.L., 2010. Development of the SAPRC-07 chemical mechanism, *Atmos. Environ.* 44, 5324–5335,
384 <https://doi.org/10.1016/j.atmosenv.2010.01.026>.
- 385 Chang, T.Y. and Rudy, S.J., 1990. Ozone-forming potential of organic emissions from alternative-fueled vehicles,
386 *Atmos. Environ.*, 24, 2421–2430, [https://doi.org/10.1016/0960-1686\(90\)90335-K](https://doi.org/10.1016/0960-1686(90)90335-K).

387 Chen, L., Zhu, J., Liao, H., Yang, Y., Yue, X., 2020. Meteorological influences on PM_{2.5} and O₃ trends and
388 associated health burden since China's clean air actions, *Sci. Total Environ.* 744, 140837,
389 <https://doi.org/10.1016/j.scitotenv.2020.140837>.

390 Dai, P., Ge, Y., Lin, Y., Su, S., and Liang, B., 2013. Investigation on characteristics of exhaust and evaporative
391 emissions from passenger cars fueled with gasoline/methanol blends. *Fuel.* 113, 10–16.

392 Deng, C. X., Jin, Y. J., Zhang, M., Liu, X. W., Yu, Z.M., 2018. Emission Characteristics of VOCs from On-Road
393 Vehicles in an Urban Tunnel in Eastern China and Predictions for 2017–2026. *Aerosol Air Qual. Res.* 18, 3025–
394 3034.

395 Doumbia, T., Granier, C., Elguindi, N., Bouarar, I., Darras, S., Brasseur, G., Gaubert, B., Liu, Y., Shi, X.,
396 Stavrakou, T., Tilmes, S., Lacey, F., Deroubaix, A., Wang, T., 2021. Changes in global air pollutant emissions
397 during the COVID-19 pandemic: a dataset for atmospheric modeling. *Earth Syst. Sci. Data.* 13, 4191–4206.

398 Fan, H., Zhao, C., Yang, Y., 2020. A Comprehensive Analysis of the Spatio-Temporal Variation of Urban Air
399 Pollution in China During 2014–2018, *Atmos. Environ.*, 220, 117066,
400 <https://doi.org/10.1016/j.atmosenv.2019.117066>.

401 Feng, J., Liao, H., Li, Y., Zhang, Z., Tang, Y., 2020. Long-term trends and variations in haze-related weather
402 conditions in north China during 1980–2018 based on emission-weighted stagnation intensity. *Atmos. Environ.*
403 240, 117830, <https://doi.org/10.1016/j.atmosenv.2020.117830>.

404 Fu, Y., Liao, H., Yang, Y., 2019. Interannual and Decadal Changes in Tropospheric Ozone in China and the
405 Associated Chemistry Climate Interactions: A Review, *Adv. Atmos. Sci.* 36, 975–993.

406 Gani, S., Bhandari, S., Seraj, S., Wang, D. S., Patel, K., Soni, P., Arub, Z., Habib, G., Hildebrandt Ruiz, L., Apte,
407 J. S., 2019. Submicron aerosol composition in the world's most polluted megacity: the Delhi Aerosol Supersite
408 study. *Atmos. Chem. Phys.* 19, 6843–6859.

409 Grosjean, D., and Seinfeld, J. H., 1989. Parameterization of the formation potential of secondary organic aerosols,
410 *Atmos. Environ.*, 23, 1733-1747, 10.1016/0004- 6981(89)90058-9.

411 Guenther, A.B., Zimmerman, P.R., Harley, P.C., Monson, R.K., Fall, R., 1993. Isoprene and monoterpene
412 emission rate variability: Model evaluations and sensitivity analyses. *J. Geophys. Res. Atmos.* 98, 12609–12617,
413 <https://doi.org/10.1029/93JD00527>.

414 Han, S., Zhao, Q., Zhang, R., Liu, Y., Li, C., Zhang, Y., Li, Y., Yin, S., Yan, Q., 2020. Emission characteristic
415 and environmental impact of process-based VOCs from prebaked anode manufacturing industry in Zhengzhou,
416 China. *Atmos. Pollut. Res.* 627 11, 67-77, 10.1016/j.apr.2019.09.016.

417 Hanna, S. R., Moore, G. E., Fernau, M., 1996. Evaluation of photochemical grid models (UAM-IV, UAM-V,
418 and the ROM/UAMIV couple) using data from the Lake Michigan Ozone Study (LMOS). *Atmos. Environ.* 30,
419 3265–3279.

420 Hong, Z., Li, M., Wang, H., Xu, L., Hong, Y., Chen, J., Chen, J., Zhang, H., Zhang, Y., Wu, X., Hu, B., Li, M.,
421 2019. Characteristics of atmospheric volatile organic compounds (VOCs) at a mountainous forest site and two
422 urban sites in the southeast of China. *Sci. Total. Environ.* 657, 1491–1500,
423 <https://doi.org/10.1016/j.scitotenv.2018.12.132>.

424 Huang, R.J., Zhang, Y., Bozzetti, C., Ho, K.F., Cao, J.J., Han, Y., Daellenbach, K. R., Slowik, J. G., Platt, S. M.,
425 Canonaco, F., Zotter, P., Wolf, R., Pieber, S. M., Bruns, E. A., Crippa, M., Ciarelli, G., Piazzalunga, A.,
426 Schwikowski, M., Abbaszade, G., Schnelle-Kreis, J., Zimmermann, R., An, Z., Szidat, S., Baltensperger, U., El

427 Haddad, I., Prevot, A.S.H., 2014. High secondary aerosol contribution to particulate pollution during haze events
428 in China, *Nature*, 514, 218-222, 10.1038/nature13774.

429 Jobson, B. T., Berkowitz, C. M., Kuster, W. C., Goldan, P. D., Williams, E. J., Fesenfeld, F. C., Apel, E. C., Karl,
430 T., Lonneman, W. A., Riemer, D., 2004. Hydrocarbon source signatures in Houston, Texas: Influence of the
431 petrochemical industry. *J. Geophys. Res. Atmos.* 109, D24305, <https://doi.org/10.1029/2004jd004887>.

432 Kuang, Y., He, Y., Xu, W.Y., Yuan, B., Zhang, G., Ma, Z.Q., Wu, C.H., Wang, C.M., Wang, S.H., Zhang, H.Y.,
433 Tao, J.C., Ma, N., Su, H., Cheng, Y.F., Shao, M., Sun, Y.L., 2020. *Environ Sci & Technol.* 54 (7), 3849-3860.

434 Li, L., Chen, Y., Zeng, L., Shao, M., Xie, S., Chen, W., Lu, S., Wu, Y., Cao, W., 2014. Biomass burning
435 contribution to ambient volatile organic compounds (VOCs) in the Chengdu–Chongqing Region (CCR), China.
436 *Atmos. Environ.* 99, 403–410.

437 Li, J., Xie, S.D., Zeng, L.M., Li, L.Y., Li, Y.Q., Wu, R.R., 2015. Characterization of ambient volatile organic
438 compounds and their sources in Beijing, before, during, and after Asia-Pacific Economic Cooperation China
439 2014. *Atmos. Chem. Phys.* 15, 7945–7959

440 Li, G., Bei, N., Cao, J., Wu, J., Long, X., Feng, T., Dai, W., Liu, S., Zhang, Q., Tie, X., 2017a. Widespread and
441 persistent ozone pollution in eastern China during the non-winter season of 2015: observations and source
442 attributions, *Atmos. Chem. Phys.*, 17, 2759–2774, <https://doi.org/10.5194/acp-17-2759-2017>.

443 Li, Y. J., Sun, Y., Zhang, Q., Li, X., Li, M., Zhou, Z., Chan, C. K., 2017b. Real-time chemical characterization
444 of atmospheric particulate matter in China: A review, *Atmos. Environ.*, 158, 270–304.

445 Li, B., Ho, S.S.H., Gong, S., Ni, J., Li, H., Han, L., Yang, Y., Qi, Y., Zhao, D., 2019a. Characterization of VOCs
446 and their related atmospheric processes in a central Chinese city during severe ozone pollution periods. *Atmos.*
447 *Chem & Phys.* 19, 617-638.

448 Li, K., Jacob, D.J., Liao, H., Shen, L., Zhang, Q., Bates, K.H., 2019c. Anthropogenic Drivers of 2013–2017
449 Trends in Summer Surface Ozone in China. *Proc. Natl. Acad. Sci.* 116, 422–427.

450 Li, K., Li, J., Tong, S., Wang, W., Huang, R.-J., Ge, M., 2019d. Characteristics of wintertime VOCs in suburban
451 and urban Beijing: concentrations, emission ratios, and festival effects. *Atmos. Chem & Phys.* 19, 8021-8036.

452 Li, K., Jacob, D.J., Shen, L., Lu, X., De Smedt, I., Liao, H., 2020. Increases in surface ozone pollution in China
453 from 2013 to 2019: anthropogenic and meteorological influences. *Atmos. Chem & Phys.* 20, 11423-11433.

454 Liang, Y., Liu, X., Wu, F., Guo, Y., Xiao, H., 2020. The year-round variations of VOC mixing ratios and their
455 sources in Kuytun City (northwestern China), near oilfields. *Atmos. Pollut. Res.* 11,9
456 DOI:10.1016/j.apr.2020.05.022.

457 Liu, B., Liang, D., Yang, J., Dai, Q., Bi, X., Feng, Y., Yuan, J., Xiao, Z., Zhang, Y., Xu, H., 2016a.
458 Characterization and source apportionment of volatile organic compounds based on 1-year of observational data
459 in Tianjin, China. *Environ. Pollut.* 218, 757–769, <https://doi.org/10.1016/j.envpol.2016.07.072>.

460 Liu, B. S., Liang, D. N., Yang, J. M., Dai, Q. L., Bi, X. H., Feng, Y. C., Yuan, J., Xiao, Z. M., Zhang, Y. F., and
461 Xu, H., 2019b. Characterization and source apportionment of volatile organic compounds based on 1-year of
462 observational data in Tianjin, China. *Environ. Pollut.* 218, 757–769.

463 Liu, Y., Wang, H., Jing, S., Gao, Y., Peng, Y., Lou, S., Cheng, T., Tao, S., Li, L., Li, Y., 2019. Characteristics
464 and sources of volatile organic compounds (VOCs) in Shanghai during summer: Implications of regional
465 transport. *Atmospheric Environment* 215, 116902.

466 Liu, Y.F., Song, M.D., Liu, X.G., Zhang, Y.P., Hui, L.R., Kong, L.W., Zhang, Y.Y., Zhang, C., Qu, Y., An, J.L.,
467 Ma, D.P., Tan, Q.W., Feng, M., 2020a. Characterization and sources of volatile organic compounds (VOCs) and
468 their related changes during ozone pollution days in 2016 in Beijing, China. *Environ Pollut.* 257, 113599.

469 Liu, Y.M., Wang, T., 2020b. Worsening urban ozone pollution in China from 2013 to 2017–Part 2: The effects
470 of emission changes and implications for multi-pollutant control. *Atmos. Chem. Phys.* 20, 6323–6337.

471 Liu, C., Shi, K., 2021. A review on methodology in O₃-NO_x-VOC sensitivity study. *Environmental pollution*,
472 118249.

473 Lu, X., Zhang, L., Wang, X., Gao, M., Li, K., Zhang, Y., Yue, X., Zhang, Y., 2020. Rapid increases in warm-
474 season surface ozone and resulting health impact in China since 2013. *Environ. Sci & Technol Lett.* 7, 240-247.

475 McDonald, B.C., de Gouw, J.A., Gilman, J.B., Jathar, S.H., Akherati, A., Cappa, C.D., Jimenez, J.L., Lee-Taylor,
476 J., Hayes, P.L., McKeen, S.A., Cui, Y.Y., Kim, S.W., Gentner, D.R., Isaacman-VanWertz, G., Goldstein, Allen
477 H., Harley, R.A., Frost, G.J., Roberts, J. M., Ryerson, T.B., Trainer, M., 2018. Volatile chemical products
478 emerging as largest petrochemical source of urban organic emissions, *Science*, 359, 760,
479 <https://doi.org/10.1126/science.aag0524>.

480 McGaughey, G. R., Desai, N. R., Allen, D. T., Seila, R.L., Lonneman, W. A., Fraser, M. P., Harley, R. A., Pollack,
481 A. K., Ivy, J. M., Price, J. H., 2004. Analysis of motor vehicle emissions in a Houston tunnel during the TexasAir
482 Quality Study 2000. *Atmos. Environ.* 38, 3363 – 3372.

483 Miller, L., Xu, X., Grgicak-Mannion, A., Brook, J., Wheeler, A., 2012. Multi-season, multiyear concentrations
484 and correlations amongst the BTEX group of VOCs in an urbanized industrial city. *Atmos. Environ.* 61, 305–
485 315.

486 Mo, Z., Shao, M., Lu, S., Qu, H., Zhou, M., Sun, J., Gou, B., 2015. Process-specific emission characteristics of
487 volatile organic compounds (VOCs) from petrochemical facilities in the Yangtze River Delta, China. *Sci. Total
488 Environ.* 533, 422–431.

489 Mo, Z., Shao, M., Lu, S., 2016. Compilation of a source profile database for hydrocarbon and OVOC emissions
490 in China. *Atmos. Environ.* 143, 209–217.

491 Odum, J.R., Jungkamp, T.P.W., Griffifin, R.J., Flagan, R.C., Seinfeld, J.H., 1997. The atmospheric aerosol-
492 forming potential of whole gasoline vapor. *Science.* 276, 96–99.

493 Peng, J., Hu, M., Shang, D., Wu, Z., Du, Z., Tan, T., Wang, Y., Zhang, F., Zhang, R., 2021. Explosive secondary
494 aerosol formation during severe haze in the North China Plain. *Environ Sci & Technol.* 55, 2189-2207.

495 Polissar, A.V., Hopke, P.K., Paatero, P., Kaufmann, Y.J., Hall, D.K., Bodhaine, B.A., Dutton, E.G., Harris, J.M.,
496 1999. The aerosol at Barrow, Alaska: long-term trends and source locations. *Atmos. Environ.* 33, 2441–2458,
497 [https://doi.org/10.1016/S1352-2310\(98\)00423-3](https://doi.org/10.1016/S1352-2310(98)00423-3), 1999.

498 Qiao, Y.Z., Wang, H.L., Huang, C., Chen, C.H., Su, L.Y., Zhou, M., Xu, H., Zhang, G.F., Chen, Y.R., Li, L., Chen,
499 M.H., Huang, H.Y., 2012. Source Profile and Chemical Reactivity of VolatileOrganic Compounds from Vehicle
500 Exhaust. *Huanjing Kexue.* 33,1071–1079.

501 Raysoni, A.U., Stock, T.H., Sarnat, J.A., Chavez, M.C., Sarnat, S.E., Montoya, T., Holguin, F., Li, W.W., 2017.
502 Evaluation of VOC concentrations in indoor and outdoor microenvironments at near-road schools. *Environ.*
503 *Pollut.* 231, 681–693.

504

505 Russo, R. S., Zhou, Y., White, M. L., Mao, H., Talbot, R., Sive, B. C., 2010. Multi-year (2004–2008) record of
506 nonmethane hydrocarbons and halocarbons in New England: seasonal variations and regional sources. *Atmos.*
507 *Chem. Phys.* 10, 4909–4929.

508 Sato, K., Takami, A., Isozaki, T., Hikida, T., Shimono, A., Imamura, T., 2010. Mass spectrometric study of
509 secondary organic aerosol formed from the photo-oxidation of aromatic hydrocarbons. *Atmos. Environ.* 44,
510 1080–1087, <https://doi.org/10.1016/j.atmosenv.2009.12.013>.

511 Shao, M., Zhang, Y., Zeng, L., Tang, X., Zhang, J., Zhong, L., Wang, B., 2009. Ground-level ozone in the Pearl
512 River Delta and the roles of VOC and NO_x in its production. *J. Environ. Manage.* 90, 512-518.

513 She, Q., Choi, M., Belle, J. H., Xiao, Q., Bi, J., Huang, K., Meng, X., Geng, G., Kim, J., He, K., Liu, M., Liu, Y.,
514 2020. Satellite-based estimation of hourly PM_{2.5} levels during heavy winter pollution episodes in the Yangtze
515 River Delta, China. *Chemosphere.* 239, 124678, <https://doi.org/10.1016/j.chemosphere.2019.124678>.

516 Shen, L., Jacob, D. J., Liu, X., Huang, G., Li, K., Liao, H., Wang, T., 2019. An evaluation of the ability of the
517 Ozone Monitoring Instrument (OMI) to observe boundary layer ozone pollution across China: application to
518 2005–2017 ozone trends. *Atmos. Chem. Phys.* 19, 6551–6560, <https://doi.org/10.5194/acp-19-6551-2019>.

519 Shen, L., Wang, Z., Cheng, H., Liang, S., Xiang, P., Hu, K., Yin, T., Yu, J., 2020. A Spatial-Temporal Resolved
520 Validation of Source Apportionment by Measurements of Ambient VOCs in Central China, *Int. J. Env. Res. Pub.*
521 *He.* 17, 791, <https://doi.org/10.3390/ijerph17030791>.

522 Shi, J., Deng, H., Bai, Z., Kong, S., Wang, X., Hao, J., Han, X., Ning, P., 2015. Emission and profile characteristic
523 of volatile organic compounds emitted from coke production, iron smelt, heating station and power plant in
524 Liaoning Province, China. *Sci. Total Environ.* 515, 101–108.

525 Sillman, S., 1999. The relation between ozone, NO_x and hydrocarbons in urban and polluted rural environments,
526 *Atmos. Environ.*, 33, 1821–1845, 1999.

527 Sindelarova, K., Markova, J., Simpson, D., Huszar, P., Karlicky, J., Darras, S., Granier, C., 2022. High-resolution
528 biogenic global emission inventory for the time period 2000–2019 for air quality modelling. *Earth Syst. Sci. Data.*
529 14, 251–270.

530 Sinha, B.P. and Sinha, V., 2019. Source apportionment of volatile organic compounds in the northwest Indo-
531 Gangetic Plain using a positive matrix factorization model. *Atmos. Chem. Phys.* 19, 15467–15482.

532 Song, M.D., Li, X., Yang, S.D., Yu, X.A., Zhou, S.X., Yang, Y.M., Chen, S.Y., Dong, H.B., Liao, K.R., Chen,
533 Q., Lu, K.D., Zhang, N.N., Cao, J.J., Zeng, L.M., Zhang, Y.H., 2021. Spatiotemporal variation, sources, and
534 secondary transformation potential of volatile organic compounds in Xi'an, China. *Atmos. Chem. Phys.* 21,
535 4939–4958.

536 Stavrakou, T., Müller, J.-F., Bauwens, M., De Smedt, I., Van Roozendael, M., Guenther, A., Wild, M., Xia, X.,
537 2014. Isoprene emissions over Asia 1979–2012: impact of climate and land-use changes. *Atmos. Chem. Phys.*
538 14, 4587–4605, <https://doi.org/10.5194/acp-14-4587-2014>.

539 Sun, W., Wang, D., Yao, L., Fu, H., Fu, Q., Wang, H., Li, Q., Wang, L., Yang, X., Xian, A. (2019) Chemistry-
540 triggered events of PM_{2.5} explosive growth during late autumn and winter in Shanghai, China. *Environmental*
541 *pollution.* 254, 112864.

542 Sun, Y. L., He, Y., Kuang, Y., Xu, W. Y., Song, S. J., Ma, N., Tao, J. C., Cheng, P., Wu, C., Su, H., Cheng, Y. F.,
543 Xie, C. H., Chen, C., Lei, L., Qiu, Y. M., Fu, P. Q., Croteau, P., Worsnop, D. R., 2020. Chemical Differences
544 Between PM₁ and PM_{2.5} in Highly Polluted Environment and Implications in Air Pollution Studies. *Geophys.*
545 *Res. Lett.* 47, No. e2019GL086288.

546 Tsai, S. M., Zhang, J. J., Smith, K. R., Ma, Y., Rasmussen, R. A., Khalil, M. A. K., 2003. Characterization of
547 Non-methane Hydrocarbons Emitted from Various Cookstoves Used in China. *Environ. Sci. Technol.* 37, 2869–

548 2877.

549 Tong, Y., Pospisilova, V., Qi, L., Duan, J., Gu, Y., Kumar, V., Rai, P., Stefenelli, G., Wang, L., Wang, Y., Zhong,
550 H., Baltensperger, U., Cao, J., Huang, R.J., Prévôt, A. S. H., Slowik, J. G., 2021. Quantification of solid fuel
551 combustion and aqueous chemistry contributions to secondary organic aerosol during wintertime haze events in
552 Beijing. *Atmos. Chem. Phys.* 21, 9859–9886.

553 Wang, H.L., Chen, C.H., Wang, Q., Huang, C., Su, L.Y., Huang, H.Y., Lou, S.R., Zhou, M., Li, L., Qiao, L.P.,
554 Wang, Y.H., 2013a. Chemical loss of volatile organic compounds and its impact on the source analysis through
555 a two-year continuous measurement. *Atmos. Environ.* 80, 488–498.

556 Wang, M., Shao, M., Lu, S.H., Yang, Y.D., Chen, W.T., 2013b. Evidence of coal combustion contribution to
557 ambient VOCs during winter in Beijing. *Chin. Chem. Lett.* 24, 829–832.

558 Wang, J., Jin, L., Gao, J., Shi, J., Zhao, Y., Liu, S., Jin, T., Bai, Z., Wu, C.Y., 2013c. Investigation of speciated
559 VOC in gasoline vehicular exhaust under ECE and EUDC test cycles. *Sci. Total Environ.* 445, 110–116.

560 Wang, Y.S., Yao, L., Wang, L.L., Liu, Z.R., Ji, D.S., Tang, G. Q., Zhang, J.K., Sun, Y., Hu, B., Xin, J.Y., 2014a.
561 Mechanism for the formation of the January 2013 heavy haze pollution episode over central and eastern China.
562 *Sci. China Earth Sci.* 57, 14–25, <https://doi.org/10.1007/s11430-013-4773-4>.

563 Wang, H., Qiao, Y., Chen, C., Lu, J., Dai, H., Qiao, L., Lou, S., Huang, C., Li, L., Jing, S., Wu, J., 2014b. Source
564 Profiles and Chemical Reactivity of Volatile Organic Compounds from Solvent Use in Shanghai, China. *Aerosol*
565 *Air Qual. Res.* 14, 301–310.

566 Wang, T., Xue, L., Brimblecombe, P., Lam, Y.F., Li, L., Zhang, L., 2017. Ozone Pollution in China: A Review
567 of Concentrations, Meteorological Influences, Chemical Precursors, and Effects. *Sci. Total Environ.* 575,
568 1582–1596.

569 Wang, J., Yang, Y., Zhang, Y., Niu, T., Jiang, X., Wang, Y., Che, H., 2019. Influence of meteorological
570 conditions on explosive increase in O₃ concentration in troposphere. *Sci.Total Environ.* 652, 1228-1241.

571 Wang, M, L., Li, S.Y., Zhu, R.C., Zhang, R.Q., Zu, L., Wang, Y.J., Bao, X.F., 2020. On-road tailpipe emission
572 characteristics and ozone formation potentials of VOCs from gasoline, diesel and liquefied petroleum gas fueled
573 vehicles. *Atmos. Environ.* 223, 117294.

574 Warneke, C., McKeen, S. A., de Gouw, J. A., Goldan, P. D., Kuster, W. C., Holloway, J. S., Williams, E. J.,
575 Lerner, B. M., Parrish, D. D., Trainer, M., Fehsenfeld, F. C., Kato, S., Atlas, E. L., Baker, A., Blake, D. R., 2007.
576 Determination of urban volatile organic compound emission ratios and comparison with an emissions database.
577 *J. Geophys. Res.* 112, D10S47, <https://doi.org/10.1029/2006jd007930>.

578 Wu, R.R., Li, J., Hao, Y.F., Li, Y.Q., Zeng, L.M., Xie, S.D., 2016. Evolution process and sources of ambient
579 volatile organic compounds during a severe haze event in Beijing, China. *Sci. Total. Environ.* 560-561, 62-72.

580 Wu, R. and Xie, S., 2018. Spatial Distribution of Secondary Organic Aerosol Formation Potential in China
581 Derived from Speciated Anthropogenic Volatile Organic Compound Emissions, *Environ. Sci. Technol.* 52,
582 8146–8156, <https://doi.org/10.1021/acs.est.8b01269>.

583 Xing, J., Wang, S. X., Jang, C., Zhu, Y., Hao, J. M., 2011. Nonlinear response of ozone to precursor emission
584 changes in China: a modeling study using response surface methodology. *Atmos. Chem. Phys.* 11, 5027–5044.

585 Xu, W., Sun, Y., Wang, Q., Zhao, J., Wang, J., Ge, X., Xie, C., Zhou, W., Du, W., Li, J., Fu, P., Wang, Z., Worsnop,
586 D.R., Coe, H., 2019. Changes in Aerosol Chemistry From 2014 to 2016 in Winter in Beijing: Insights From High-
587 Resolution Aerosol Mass Spectrometry. *J. Geophys. Res.: Atmos.* 124 (2), 1132–1147

588 Xu, Q., Wang, S., Jiang, J., 2019. Nitrate dominates the chemical composition of PM_{2.5} during haze event in
589 Beijing, China. *Sci. Total. Environ.* 689:1293-1303.

590 Xue, Y., Ho, S. S. H., Huang, Y., Li, B., Wang, L., Dai, W., Cao, J., Lee, S., 2017. Source apportionment of
591 VOCs and their impacts on surface ozone in an industry city of Baoji, Northwestern China. *Sci. Rep.* 7, 9979,
592 <https://doi.org/10.1038/s41598-017-10631-4>.

593 Xue, T., Zheng, Y., Geng, G., Xiao, Q., Meng, X., Wang, M., Li, X., Wu, N., Zhang, Q., Zhu, T., 2020a.
594 Estimating Spatiotemporal Variation in Ambient Ozone Exposure during 2013–2017 Using a Data-Fusion Model.
595 *Environ Sci. Technol.* 54, 14877-14888.

596 Xue, Y., Huang, Y., Ho, S.S.H., Chen, L., Wang, L., Lee, S., Cao, J., 2020b. Origin and transformation of ambient
597 volatile organic compounds during a dust-to-haze episode in northwest China. *Atmos. Chem. Phys.* 20, 5425-
598 5436.

599 Yan, Y., Peng, L., Li, R., Li, Y., Li, L., Bai, H., 2017. Concentration, ozone formation potential and source analysis
600 of volatile organic compounds (VOCs) in a thermal power station centralized area: A study in Shuozhou, China.
601 *Environ. Pollut.* 223, 295–304.

602 Yang, W.Q., Zhang, Y.L., Wang, X.M., Li, S., Zhu, M., Yu, Q.Q., Li, G.H., Huang, Z.H., Zhang, H.N., Wu, Z.F.,
603 Song, W., Tan, J.H., Shao, M., 2018. Volatile organic compounds at a rural site in Beijing: influence of temporary
604 emission control and wintertime heating. *Atmos. Chem. Phys.* 18, 12663–12682.

605 Yao, Y.C., Tsai, J.H., Wang, I.T., 2013. Emissionsof gaseous pollutant from motorcycle powered byethanol-
606 gasoline blend. *Appl. Energy.* 102, 93–100.

607 Yao, Z., Wu, B., Shen, X., Cao, X., Jiang, X., Ye, Y., He, K., 2015. On-road emission characteristics of VOCsfrom
608 rural vehicles and their ozone formation potential in Beijing, China. *Atmos. Environ.* 105, 91–96.

609 Yao, L., Wang, D., Fu, Q., Qiao, L., Wang, H., Li, L., Sun, W., Li, Q., Wang, L., Yang, X., 2019. The effects of
610 firework regulation on air quality and public health during the Chinese Spring Festival from 2013 to 2017 in a

611 Chinese megacity. *Environ Int.* 126, 96-106.

612 Yuan, B., Shao, M., Lu, S., Wang, B., 2010. Source profiles of volatile organic compounds associated with solvent
613 use in Beijing, China. *Atmos. Environ.* 44, 1919–1926.

614 Zhai, S., Jacob, D.J., Wang, X., Shen, L., Li, K., Zhang, Y., Gui, K., Zhao, T., Liao, H., 2019. Fine particulate
615 matter (PM_{2.5}) trends in China, 2013–2018: separating contributions from anthropogenic emissions and
616 meteorology, *Atmos. Chem. Phys.* 19, 11031– 11041, <https://doi.org/10.5194/acp-19-11031-2019>.

617 Zhang, Y., Wang, X., Zhang, Z., Lu, S., Shao, M., Lee, F.S. C., Yu, J., 2013. Species profiles and normalized re
618 activity of volatile organic compounds from gasoline evaporation in China. *Atmos. Environ.* 79, 110–118.

619 Zhang, X., Xue, Z., Li, H., Yan, L., Yang, Y., Wang, Y., Duan, J., Li, L., Chai, F., Cheng, M., Zhang, W., 2017.
620 Ambient volatile organic compounds pollution in China. *J Environ. Sci.* 55, 69-75, 10.1016/j.jes.2016.05.036.

621 Zhang, Y., Li, R., Fu, H., Zhou, D., Chen, J., 2018. Observation and analysis of atmospheric volatile organic
622 compounds in a typical petrochemical area in Yangtze River Delta, China. *J. Environ. Sci.* 71, 233-248.

623 Zhao, D., Liu, G., Xin, J., Quan, J., Wang, Y., Wang, X., 2020. Haze pollution under a high atmospheric
624 oxidization capacity in summer in Beijing: insights into formation mechanism of atmospheric physicochemical
625 processes. *Atmos. Chem. Phys.* 20, 4575-4592.

626 Zhao, Q.Y., Bi, J., Liu, Q., Ling, Z.H., Shen, G.F., Chen, F., Qiao, Y.Z., Li, C.Y., Ma, Z.W., 2020. Sources of
627 volatile organic compounds and policy implications for regional ozone pollution control in an urban location of
628 Nanjing, East China. *Atmos. Chem. Phys.* 20, 3905–3919.

629 Zheng, J., Yu, Y., Mo, Z., Zhang, Z., Wang, X., Yin, S., Peng, K., Yang, Y., Feng, X., Cai, H., 2013. Industrial
630 sector-based volatile organic compound (VOC) source profiles measured in manufacturing facilities in the Pearl
631 River Delta, China. *Sci. Total Environ.* 456, 127–136.

632 Zheng, H., Kong, S., Xing, X., Mao, Y., Hu, T., Ding, Y., Li, G., Liu, D., Li, S., Qi, S., 2018. Monitoring of
633 volatile organic compounds (VOCs) from an oil and gas station in northwest China for 1 year. *Atmos. Chem.*
634 *Phys.* 18, 4567-4595.
635

Figure captions

636

637 **Figure 1.** Time series of meteorological parameters and levels of air pollutants during the sampling
638 period.

639 **Figure 2.** Comparison of the concentration and composition of major chemical groups observed in
640 2019 (this study), 2016 (Liu et al., 2020) and 2014 (Li et al., 2015).

641 **Figure 3.** The averaged levels of temperature (T), wind speed (WS), and O₃ and NO_x concentrations
642 on (a) O₃ compliance during the O₃-polluted months, (b) O₃ pollution days during the O₃-polluted
643 months, and (c) differences in VOCs mixing ratios between O₃ compliance and pollution days. The
644 averaged levels of temperature (T), wind speed (WS), relative humidity (RH), and PM_{2.5}
645 concentrations on (d) PM_{2.5} compliance during the PM_{2.5}-polluted months, (e) PM_{2.5} pollution days
646 during the PM_{2.5}-polluted months, and (f) differences in VOCs mixing ratios between PM_{2.5}
647 compliance and pollution days.

648 **Figure 4.** Statistic decomposition of meteorological and emission contribution to O₃ and PM_{2.5}
649 levels during different periods.

650 **Figure 5.** OFP and SOAFP by chemical groups during different periods.

651 **Figure 6.** Ratios of *i/n*-pentane and toluene/benzene at different PM_{2.5} and O₃ levels.

652 **Figure 7.** Source profiles of VOCs identified using the PMF model and the relative contributions of
653 the individual VOC species.

654 **Figure 8.** Contributions of each source to VOCs on (a) O₃ compliance days during the O₃-polluted
655 months, (b) O₃ pollution days during the O₃-polluted months, and during (c) the non-O₃-polluted
656 months. Contributions of each source to VOCs on (d) PM_{2.5} compliance days during the PM_{2.5}-
657 polluted months, (e) PM_{2.5} pollution days during the PM_{2.5}-polluted months, and (f) during the non-

658 PM_{2.5}-polluted months.

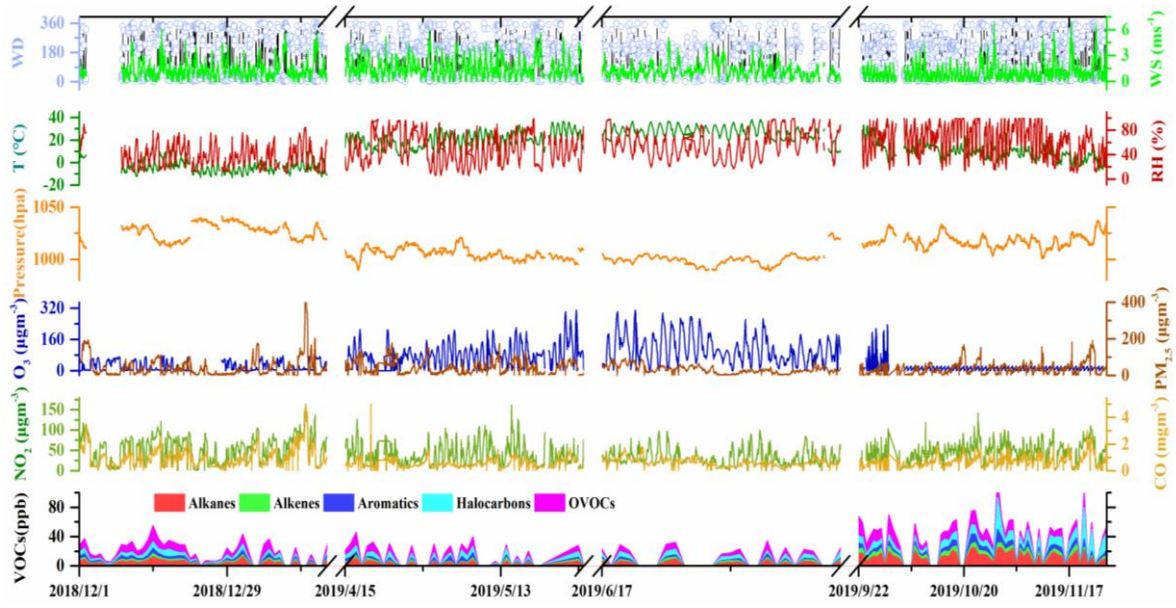
659 **Figure 9.** Contributions of each source to OFP and SOAFP during different periods.

660 **Figure 10.** OFP values of the dominant VOC species in the different source categories for the O₃

661 pollution (a) and compliance (b) days of the O₃-polluted months, and SOAFP values for the PM_{2.5}

662 pollution (c) and compliance (d) days of the PM_{2.5}-polluted months.

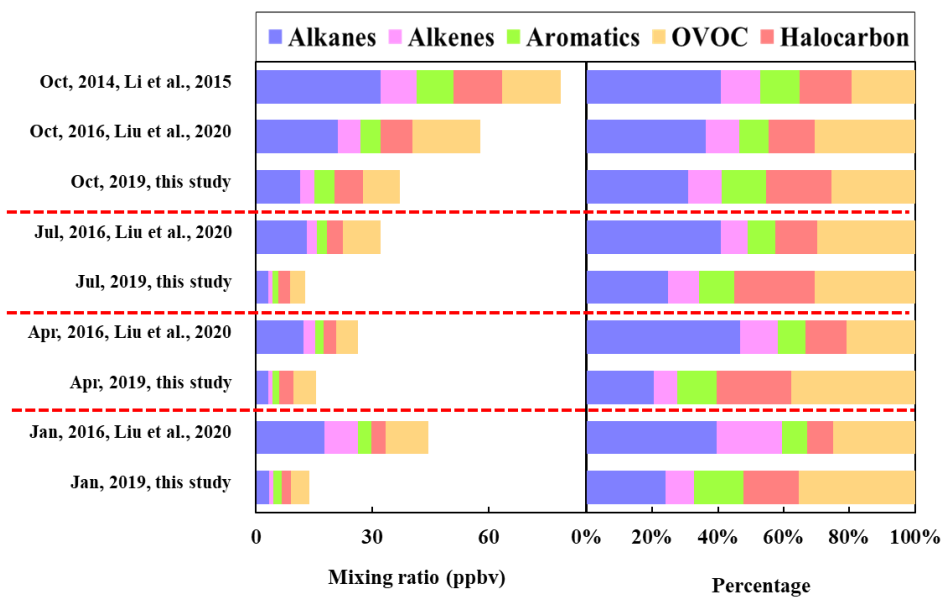
Fig. 1.



666

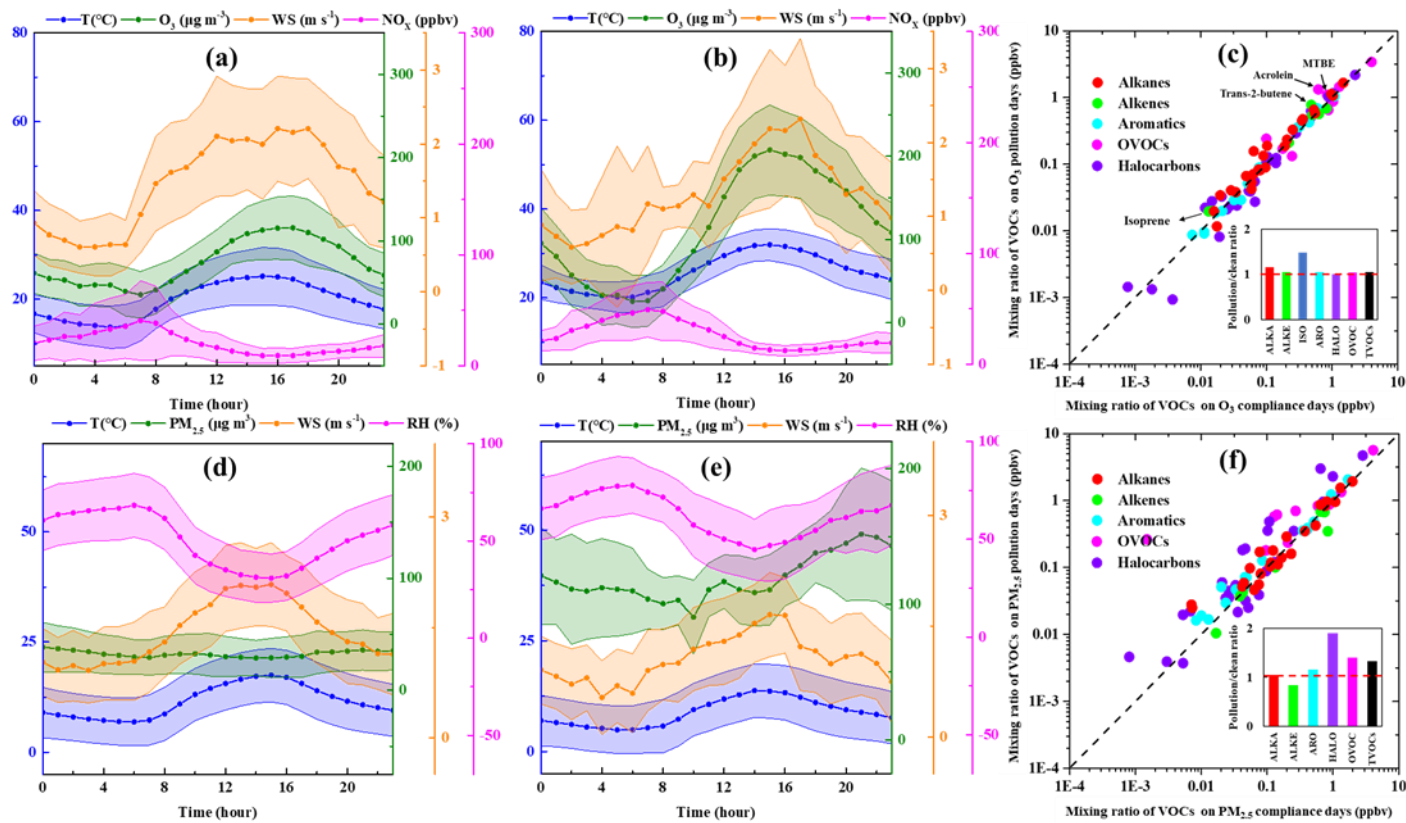
667

668 **Figure 2.**



669

670



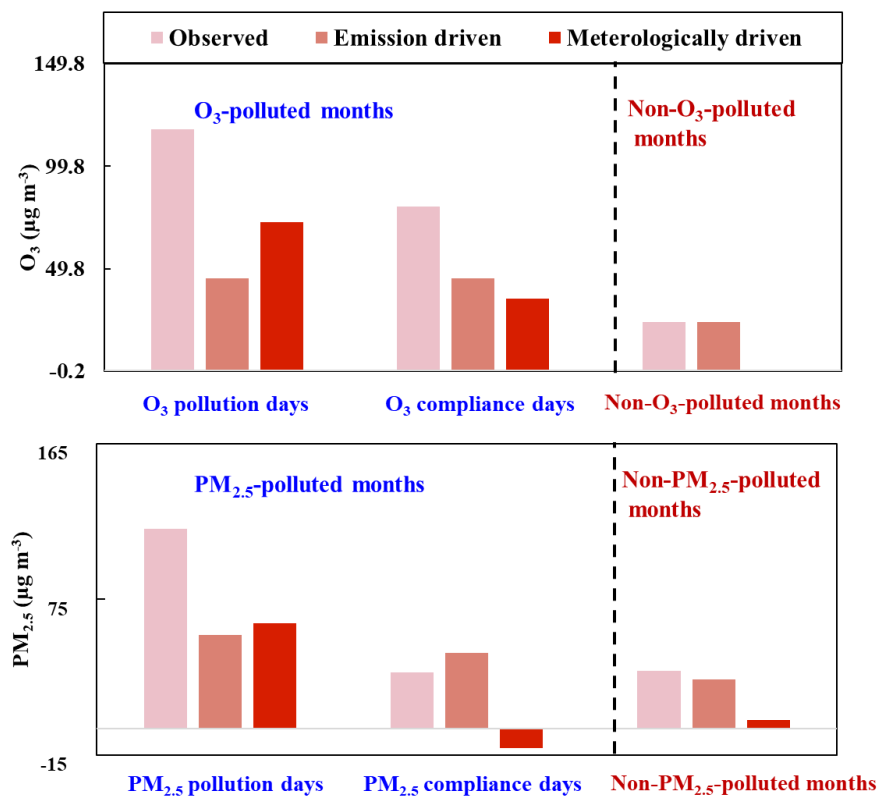
672

673

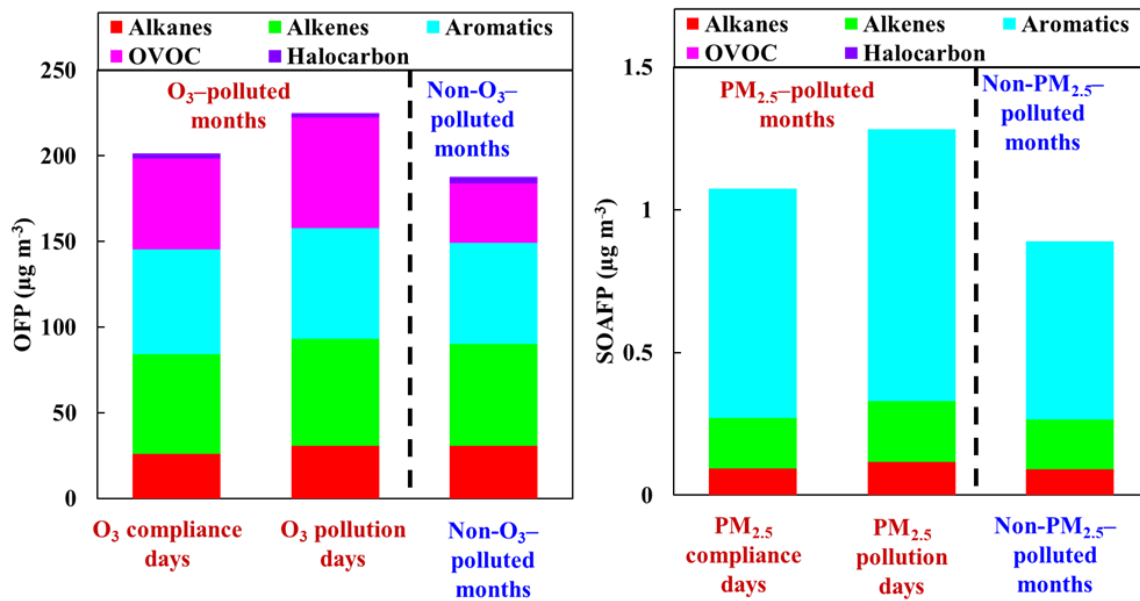
674 **Fig. 4**

675

676

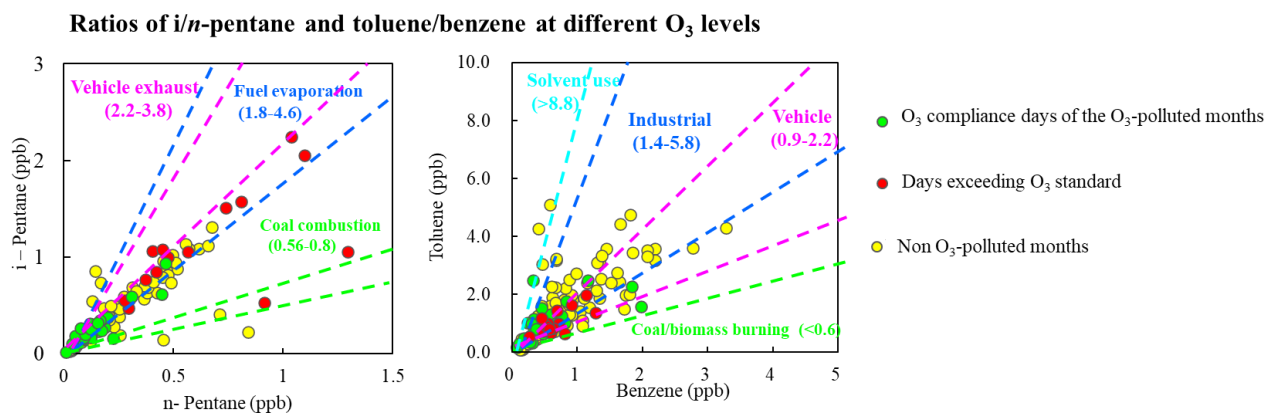
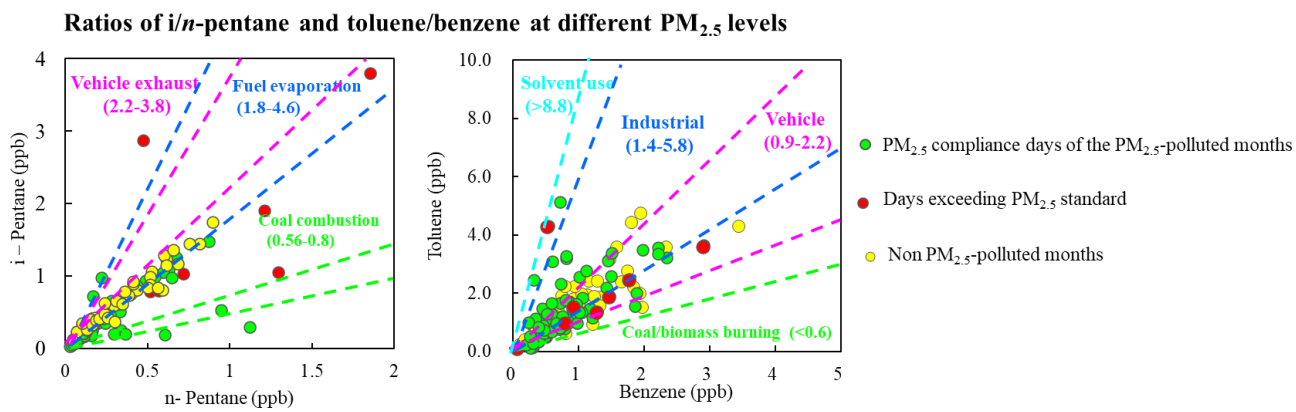


677



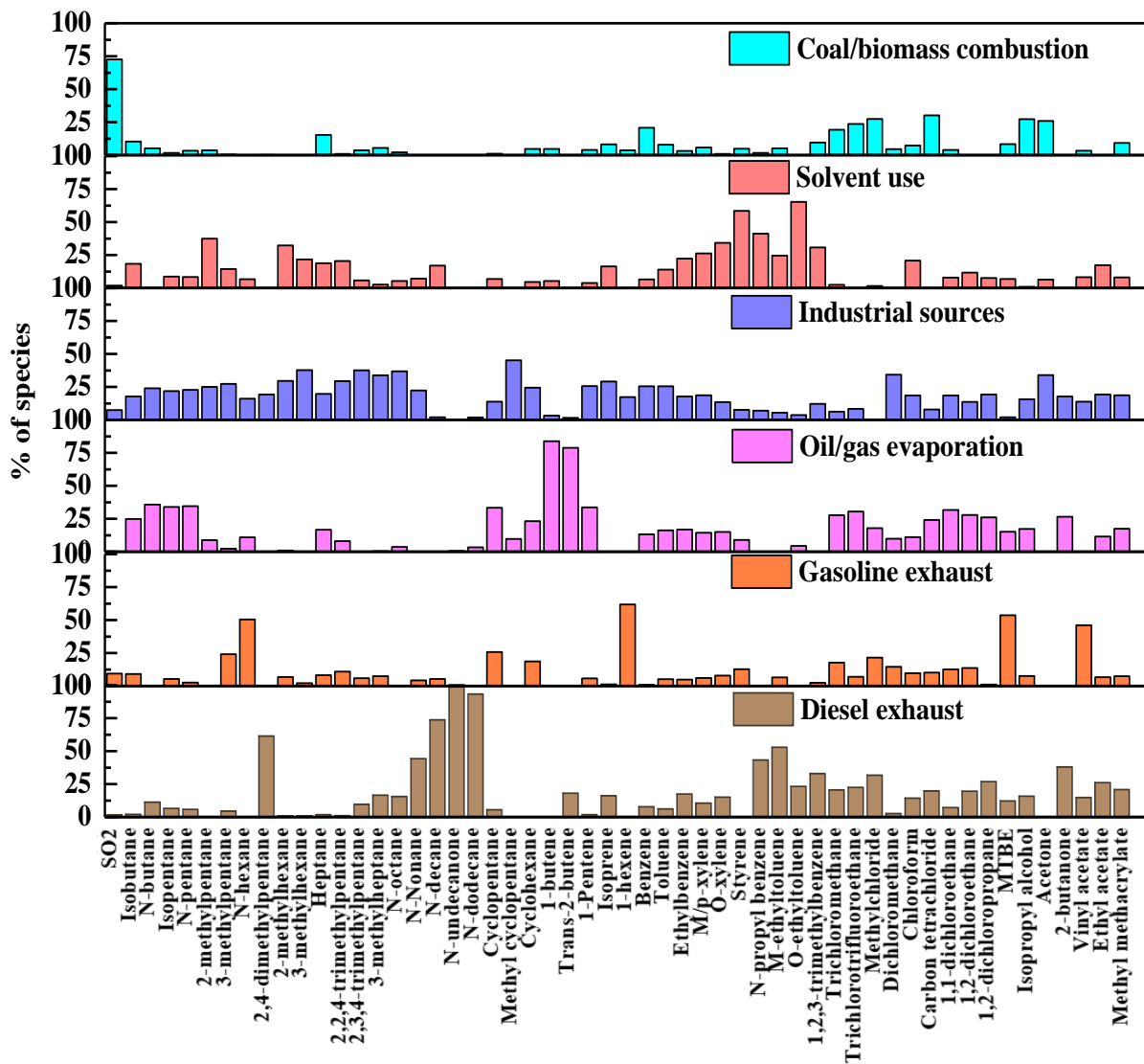
679

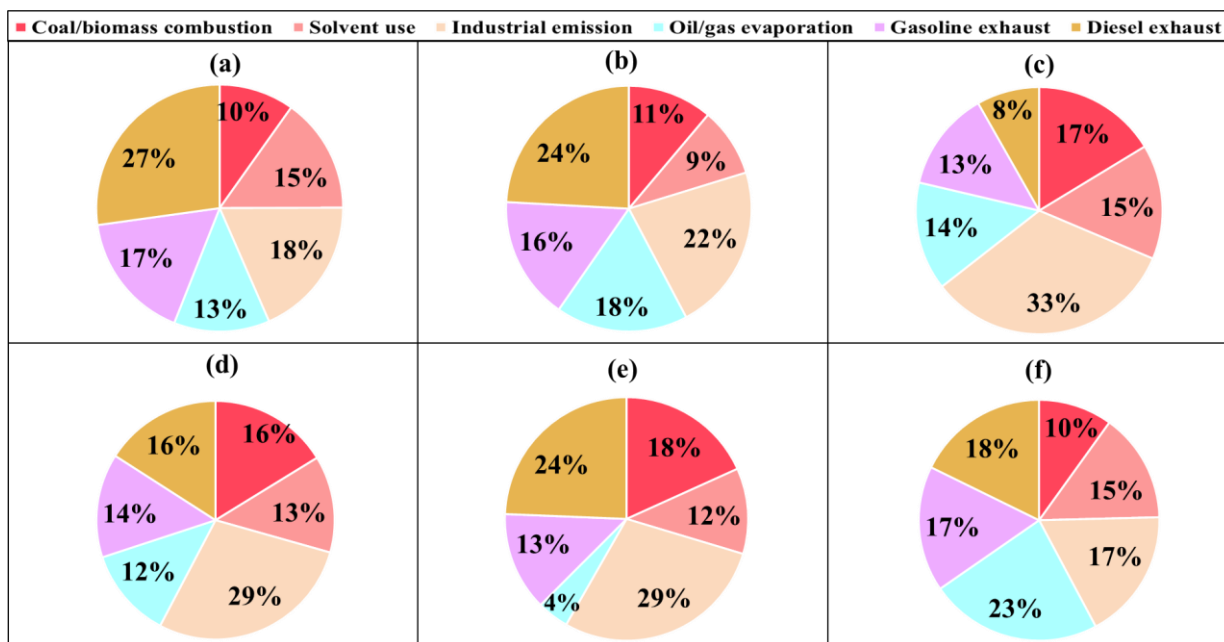
680



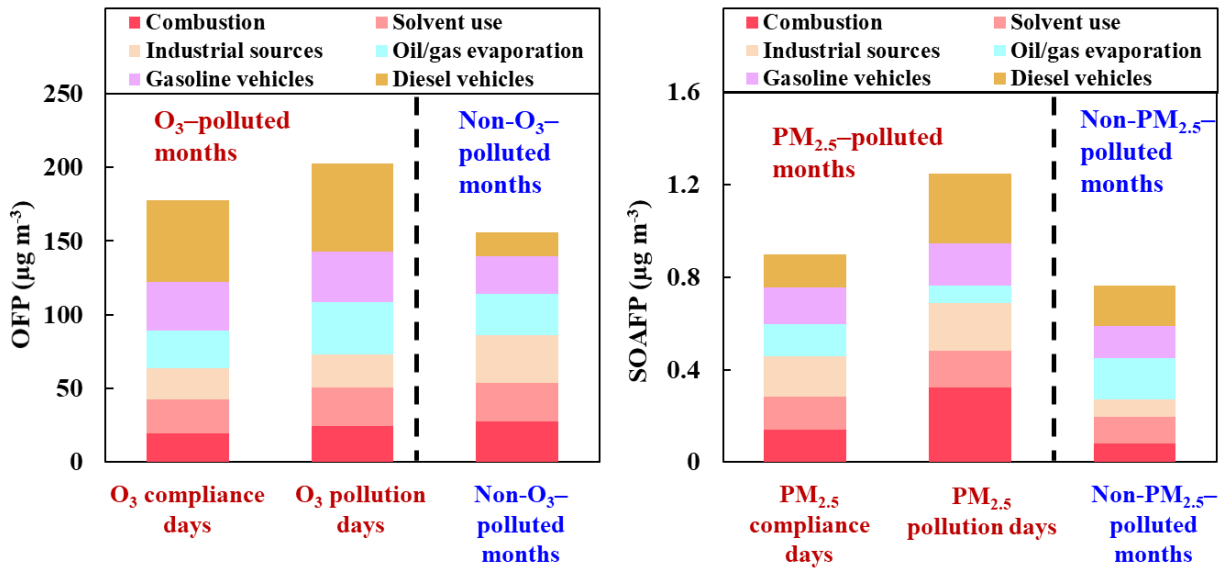
683
684
685
686
687

Fig. 7.





689
690
691



693

694

